第42卷 第9期
2015年9月

中 国 激 光
CHINESE JOURNAL OF LASERS

Vol. 42, No. 9
September, 2015

Phase Retrieval with One Interferogram by Reflecting Off-Axis Microscopic Interferometry

Zeng Yanan Lei Hai Chang Xinyu Hu Xiaodong Hu Xiaotang

State Key Laboratory of Precision Measuring Technology and Instruments, Tianjin University, Tianjin 300072, *China*

Abstract A technique called off-axis microscopic interferometry is developed to measure the surface profile of microstructures. This technique involves the use of a modified Mach-Zehnder microscopic interferometer with a tilted reference wave. The technique uses a CCD camera to record the off-axis microscopic interferogram and performs filtering in the Fourier plane via the Fourier transform method for phase retrieval. In contrast to classical microscopic interferometry, the carrier frequency of the off-axis microscopic interferogram is sufficiently high to facilitate acquisition of the phase from only one interferogram. As a result, measurements using this technique are vibration-immune and efficient. The experimental results obtained for a step height standard as well as a micro-hole array are consistent with measurements taken using a stylus profilometer. Further, the results of a comparative experiment conducted using a Mirau interferometric microscope show that the carrier frequency added to the classical microscopic interferogram cannot be as high as that of off-axis microscopic interferogram. Therefore, it will lead to incorrect phase retrieval with one interferogram.

Key words measurement; surface profile; off-axis; carrier frequency; microscopic interferometry

OCIS codes 120.3180; 180.3170; 180.6900; 120.5050

基于离轴显微干涉术的单幅干涉图相位求解

曾雅楠 雷 海 常新宇 胡晓东 胡小唐

天津大学精密测试技术及仪器国家重点实验室, 天津 300072

摘要 提出一种用于测量微结构表面形貌的离轴显微干涉术。该技术的实验装置为一个优化的马赫-曾德尔干涉仪。其特点为参考波是具有一定载频的倾斜波。该技术中应用CCD记录离轴显微干涉图,并用傅里叶变换方法对记录的干涉图在傅里叶面进行频谱滤波求解相位。不同于经典显微干涉术,离轴显微干涉图的载频较高,仅需单幅干涉图即可得到相位信息。因此该技术在测量中具有防振、快捷有效的特点。利用一个标准微台阶以及微孔阵列的形貌检测结果验证该技术的有效性,同时与轮廓仪的测试结果进行对比,证明结果一致。被测物也应用Mirau干涉显微镜进行测试,实验结果表明经典显微干涉图干涉信息载频不足,仅使用单幅干涉图不能得到正确相位,该组实验证明了离轴显微干涉术相对于传统显微干涉术的优越性。

关键词 测量; 表面形貌; 离轴; 载频; 显微干涉

中图分类号 O436.1 **文献标识码** A

doi: 10.3788/CJL201542.0908006

1 Introduction

Optical interferometry is utilized extensively in surface profile measurement because of advantages such as non-invasiveness, high precision, and full field-of-view. Optical interferometry includes techniques such as classical interferometry[1], holographic interferometry[2], electronic speckle pattern interferometry[3], and Moire interferometry[4]. Among these techniques, classical interferometry is used in Mirau, Michelson, and Linnik interferometers to test

收稿日期: 2015-02-12; **收到修改稿日期**: 2015-03-12

基金项目: 国家自然科学基金(61223008, 51375340, 51075297)

作者简介: 曾雅楠(1988—),女,博士研究生,主要从事显微干涉术方面的研究。E-mail: ynzeng@tju.edu.cn

导师简介: 胡晓东(1974—),男,博士,教授,主要从事微纳结构检测技术方面的研究。E-mail: xdhu@tju.edu.cn(通信联系人)

microstructures; for microscopic systems, microscopic interferometry is the most frequently used technique because of its good performance and simplicity[5-7]. Microscopic interferometry primarily includes phase shifting interferometry[8] and white- light scanning interferometry[9-10]. Phase shifting interferometry extracts phase from at least three inter-ferograms[11-13]. White-light scanning interferometry continually scans the surface of the sample. However, the techniques cited above have disadvantages such as necessity for several interferograms, sensitivity to vibration, and need for an expensive scanner or phase shifter with nanometer resolution. Further, the experimental configuration of an interferometer microscope requires a very high degree of precision[14]. Quantitative phase microscopy is widely utilized in the measurement of living cell movement because the phase of the samples can be retrieved using one interferogram. However, an extra microscope objective is needed in the reference arm to correct aberrations. In addition, in quantitative phase microscopy, the samples tested are rarely calibrated[15-17]. Theoretically, a combination of microscopic interferometry with the Fourier transform method would only require one interferogram. In the classical microscopic interferometry setup, this is practically achieved by tilting the tested sample to increase the carrier frequency[18-19]. However, because the carrier frequency is insufficient, phase reversal may occur because of the overlapped frequency spectrum. Consequently, an additional interferogram with a known shifted phase is usually required to correct the reversed phase[20]. Digital holographic microscopy reconstructs the wavefront of the object beam with one hologram. However, this method typically has issues such as high frequency and phase fluctuations at the edge of the reconstructed images[21-22], low efficiency resulting from the complex Fresnel diffraction-based algorithms utilized[23-25], as well as enlargement of noise levels due to diffraction calculation.

In this paper, we propose a technique based on off-axis microscopic interferometry. The approach increases the carrier frequency of the interferogram with a tilted reference beam to avoid phase reversals and corrects phase distortions. This facilitates surface profile measurement by phase retrieval from one interferogram using the filtering method in the Fourier plane via the Fourier transform method. To verify the feasibility of the proposed approach, an experimental setup that is quite similar to off- axis digital holographic microscope, only with the difference that the sample is focused by microscope objective (MO), is used. In the experiments conducted, the surface profiles of some microstructures, such as step height standard and micro-hole array, are measured to prove that the technique is feasible. Further, the results of a test conducted on the increased carrier frequency of a classical microscopic interferogram (specifically using a Mirau microscopic interferometer) by tilting the sample are presented to show that the carrier frequency is not high enough to retrieve the correct phase from one interferogram.

2 Experimental setup and principle

The experimental setup used to verify the feasibility of off-axis microscopic interferometry is shown in Fig. 1. The source was a diode pumped laser with $\lambda = 640$ nm (CrystaLaser, CL640-050-S). The object wave O containing the information about the sample was collected by MO (Mitutoyo, M Plan Apo SL, NA=0.42, magnification is $50\times$). The sample was illuminated with an approximately collimated beam by applying an object lens (OL in Fig. 1) located at the back focal plane of the MO. The reference wave R was tilted by adjusting mirror M2 to increase the carrier frequency, reducing the overlapping effect of the frequency spectrum. Like the object wave, the reference wave was also a spherical wave with the aid of the reference lens (RL in Fig. 1). The tilted angle θ, specifically the off-axis angle, is the angle between the central axis of the object and reference beams. A CCD camera (Imperx, PX-2M30-L, $M \times N = 1008 \times 1028$, square pixel view of $7.4\ \mu\mathrm{m}$, 33 frame/s) was used to record the interferogram.

The intensity distribution of the interferogram can be written as

$$i(x,y) = a(x,y) + b(x,y)\cos[\phi_{\mathrm{o}}(x,y) - \phi_{\mathrm{R}}(x,y)] = a(x,y) + c(x,y) + c^{*}(x,y)\ , \tag{1}$$

where (x,y) is the coordinate of the interferogram, $a(x,y)$ is the background intensity (which varies slowly), $b(x,y)$ is related to the local contrast of the pattern, $\phi_{\mathrm{o}}(x,y)$ is the phase of object beam at pixel (x,y), and $\phi_{\mathrm{R}}(x,y)$ is the

phase of the reference beam. The phase of $c(x,y)$ is given by

$$\phi_c(x,y)=\phi_o(x,y)-\phi_R(x,y). \tag{2}$$

The frequency spectrum of $a(x,y)$ is centralized in the adjacent domain of the origin, and the frequency spectra of $c(x,y)$ and $c^*(x,y)$ are symmetrical to the origin. $c(x,y)$ can be achieved with separation from $a(x,y)$ by adjusting mirror M2 (Fig. 1) in the off-axis setup (Fig. 1) to create a small off-axis angle θ. The angle θ is related to the spatial frequency of the interference fringes. Thus, the angle θ is evaluated as follows.

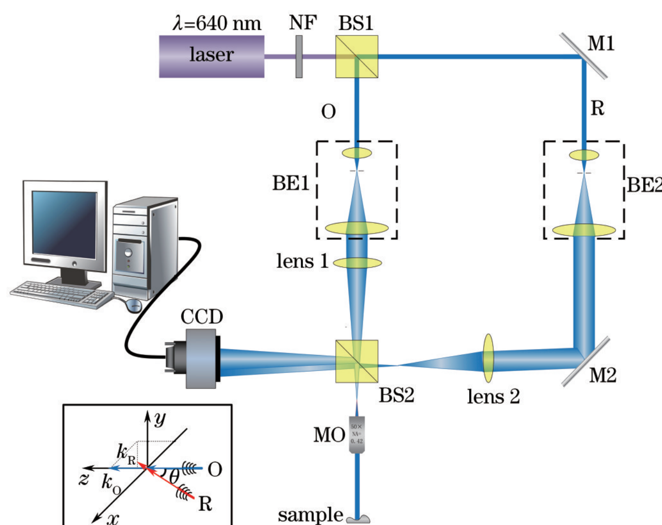

Fig.1 Off-axis microscopic interferometry in reflection configuration. NF: neutral filter; M: mirror; BE: beam expander; OL: object lens; RL: reference lens; BS: beam splitter; MO: microscope objective

The MO can be simplified as a lens. Fig. 2 shows the imaging principle of this lens.

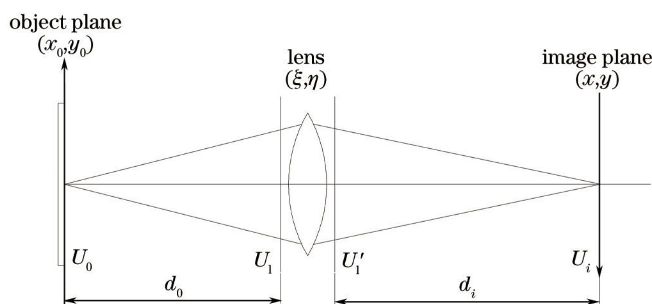

Fig.2 Imaging principle of lens

The complex amplitude distribution in the image plane is

$$\begin{aligned}U_i(x,y)=&\frac{1}{\lambda^2 d_0 d_i}\exp\left[\mathrm{j}\frac{k}{2d_i}(x^2+y^2)\right]\iint\iint U_0(x_0,y_0)P(\xi,\eta)\times\\&\exp\left(\mathrm{j}\frac{k}{2d_0}\frac{x^2+y^2}{M^2}\right)\exp\left[-\mathrm{j}\frac{k}{d_0}(x_0\xi+y_0\eta)\right]\exp\left[-\mathrm{j}\frac{k}{d_i}(x\xi+y\eta)\right]\mathrm{d}x_0\mathrm{d}y_0\mathrm{d}\xi\mathrm{d}\eta=\\&\iint D(\xi,\eta)\exp\left\{\mathrm{j}\left[\frac{-k}{d_i}(x\xi+y\eta)+\frac{k}{d_0}\left(\frac{x^2+y^2}{M^2}\right)+\frac{k}{d_i}(x^2+y^2)\right]\right\}\mathrm{d}\xi\mathrm{d}\eta\end{aligned}, \tag{3}$$

where (x_0,y_0) is the coordinate of the object plane, $U_0(x_0,y_0)$ is the object′s wavefront, (x_i,y_i) is the image plane′s coordinate, k is the wavenumber, $k=2\pi/\lambda$. λ is the wavelength of the laser source, and d_0 and d_i are the object distance and image distance, respectively. (ξ,η) is the coordinate of the lens plane, M is the imaging magnification. $c(x,y)=O(x,y)R^*(x,y)$, hence, the phase of $c(x,y)$ is

$$\phi_c(x,y) = -\frac{k}{d_i}(\xi x + \eta y) + \frac{k}{d_0}\frac{x^2+y^2}{M^2} + \frac{k}{d_i}(x^2+y^2) - \frac{k}{2d'}\left[(x-x_m)^2 + (y-y_n)^2\right], \tag{4}$$

where (x_m, y_m) is the center of the spherical reference beam, and d' is the distance from the center to the CCD camera.

Thus the spatial frequency of the fringes in the x and y directions is

$$\begin{cases} f_x = \dfrac{1}{2\pi}\dfrac{\partial P}{\partial x} = -\dfrac{k}{d_i}\xi + \dfrac{k}{d_0}\dfrac{2x}{M^2} + \dfrac{k}{d_i}2x - \dfrac{k}{2d'}(x - x_m) \\ f_y = \dfrac{1}{2\pi}\dfrac{\partial P}{\partial y} = -\dfrac{k}{d_i}\eta + \dfrac{k}{d_0}\dfrac{2y}{M^2} + \dfrac{k}{d_i}2y - \dfrac{k}{2d'}(y - y_n) \end{cases}. \tag{5}$$

The spatial frequency should not only be large enough to separate $c(x,y)$ and $c^*(x,y)$ from $a(x,y)$, but also less than the cut-off frequency of the CCD camera according to the Nyquist sampling theory. Therefore,

$$\begin{cases} (f_{x\min})_{\mathrm{OR}^*} \geqslant (f_{x\max})_{|O|^2} = \dfrac{MX}{\lambda d_i} \\ (f_{y\min})_{\mathrm{OR}^*} \geqslant (f_{y\max})_{|O|^2} = \dfrac{MY}{\lambda d_i} \\ (f_{x\min})_{\mathrm{OR}^*} \leqslant \dfrac{1}{2\Delta x} \\ (f_{x\min})_{\mathrm{OR}^*} \leqslant \dfrac{1}{2\Delta y} \end{cases}, \tag{6}$$

where X and Y are, respectively, the size of the sample in the x and y directions. Δx and Δy are the sampling intervals in the image plane, specifically, the pixel size of the CCD camera.

The off-axis angle θ is

$$\theta \approx \tan\theta = \frac{\sqrt{x_m^2 + y_n^2}}{d}, \tag{7}$$

where d is the vertical distance between mirror M2 in Fig. 1 and the center of the spherical reference beam. According to equations (6) and (7) and the parameters of the selected components in our setup, θ is evaluated in the range of $1.18°$~$1.53°$. Thus, it is set to approximately $1.5°$.

Consequently, $c(x,y)$ is obtained by frequency-domain filtering of the interferogram:

$$c(x,y) = F^{-1}\left\{D(\xi,\eta)W_i(\xi,\eta)F[I(x,y)]\right\}, \tag{8}$$

where F and F^{-1} denote Fourier transform and inverse Fourier transform, respectively. $W_i(\xi,\eta)$ is the window function for frequency filtering and $D(\xi,\eta)$ is the shifting function to shift the filtered frequency spectrum to the center. The window function is chosen to be a circular one, with center located at the most powerful point in the frequency spectrum and radius set to include as much of the frequency spectrum as possible while avoiding the central part.

The phase distortions caused by the position error between the centers of the two interfering spherical waves can be viewed as system error because they are relatively fixed if the setup is kept stationary. It is calculated by phase correction of computation related to optical aberration parameters. The phase of the reference wave and the surface profile can be calculated using equations (9) and (10), respectively.

$$\phi_{\mathrm{sample}}(x,y) = \arctan\left\{\frac{\mathrm{Im}\left[c(x,y)\times\exp(-\phi_{\mathrm{se}})\right]}{\mathrm{Re}\left[c(x,y)\times\exp(-\phi_{\mathrm{se}})\right]}\right\}, \tag{9}$$

$$h = \frac{\phi_{\mathrm{sample}}(x,y)\times\lambda}{4\pi}, \tag{10}$$

where ϕ_{se} is the phase of the system error and h is the height of the tested sample.

3 Results and analysis

To evaluate the feasibility of off-axis microscopic interferometry, the surface profiles of a nanometer step height standard [VLSI, SHS-440-QC, (43.2 ± 0.6) nm] and a micro-hole array (853 nm in depth) were measured and

analyzed. The results were compared to those obtained using a stylus profilometer (KLA−Tencor, P−16+/P−6) with a mass of 2 mg, which confirmed that the system error was effectively corrected. To evaluate whether the carrier frequency was high enough to extract phase from one interferogram in order to measure the surface profile of the complicated microstructure, the micro−hole array was also tested using a classical Mirau microscopic interferometer combined with the Fourier transform method.

Fig. 3(a) depicts one interferogram of the step height standard. The magnified section of the interferogram shows the interference fringes with high carrier frequency. Fig. 3(b) is the fast Fourier transform (FFT) frequency spectrum of the interferogram, which indicates that $c(x,y)$ can be obtained via simple window filtering and inverse FFT. Fig. 3 (c) is the measured original surface profile of the step height standard, which is incorrect because of the system error. The correct surface profile of the step height standard is obtained and shown in Fig. 3(d). The obvious noise revealed in the height figure is primarily caused by dirty spots on the sample. Fig. 3(e) is the profile line plotted along line 100 in Fig. 3(d) with a stylus profilometer and the off−axis microscopic interferometer. Following low−pass filtering of the height image to reduce the effect of noise, the flatness was calculated as 0.98 nm, which shows

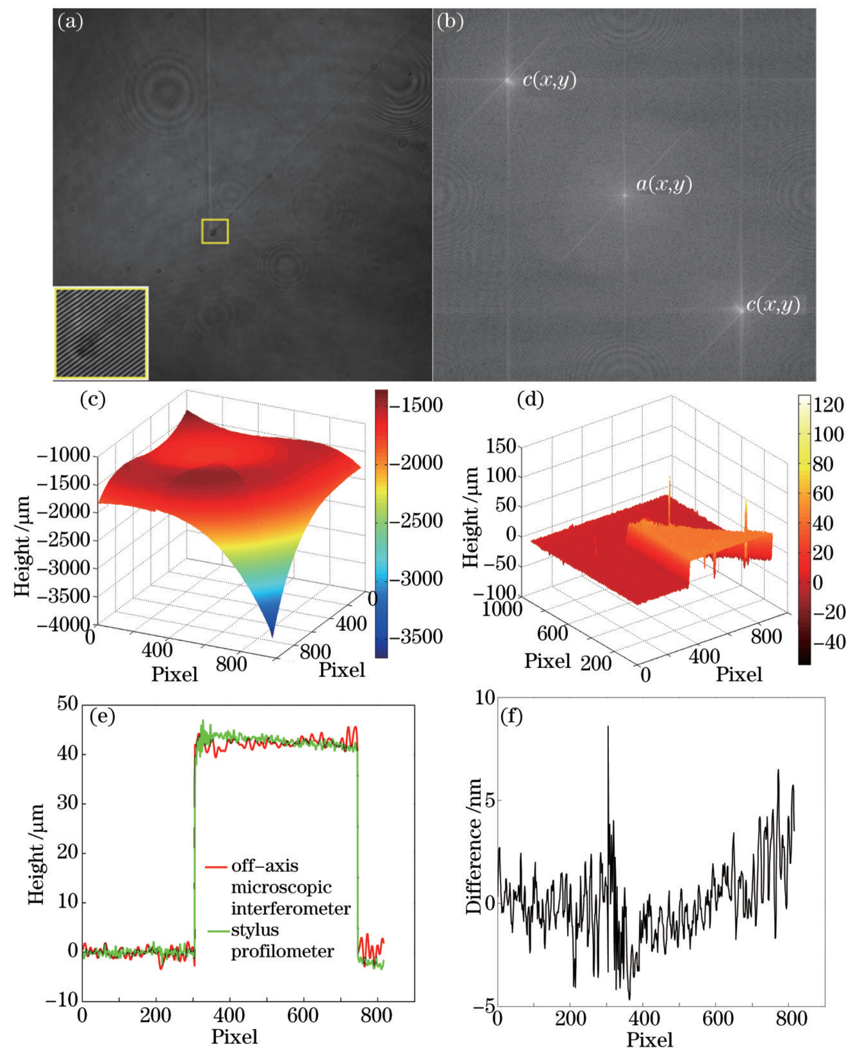

Fig.3 Experimental results of the step height standard. (a) Interferogram of the step height standard—the figure in the yellow rectangular frame is the magnified part; (b) frequency spectrum of the interferogram; (c) measured original surface profile of the step height standard without error correction; (d) correct surface profile of the step height standard; (e) profile line plotted along line 100 in Fig. 3(d) with the stylus profilometer (red line) and the off−axis microscopic interferometer (green line); (f) difference between the data obtained from the stylus profilometer and the off−axis microscopic interferometer

that the phase distortions were effectively corrected. The step height measured was (42.6 ± 0.7) nm. This is in reasonable agreement with the standard value. Fig. 3(f) shows the difference between the data obtained from the stylus profilometer and the off-axis microscopic interferometry setup. The difference is controlled in the range of −4.2~ 5.4 nm. The effective area of the field of view is approximately 149 μm×152 μm with the 50 × MO.

The results for the micro-hole array specimen are illustrated in Fig. 4. Fig. 4(a) is the interferogram of the micro-hole array. Fig. 4(b) is the correct surface profile of the sample. Fig. 4(c) shows the profile lines of the black line in Fig. 4(b), obtained by the off-axis microscopic interferometer and the stylus profilometer, which are in good agreement. The depth of the micro-hole array after multiple measurements is (850.3±3.2) nm.

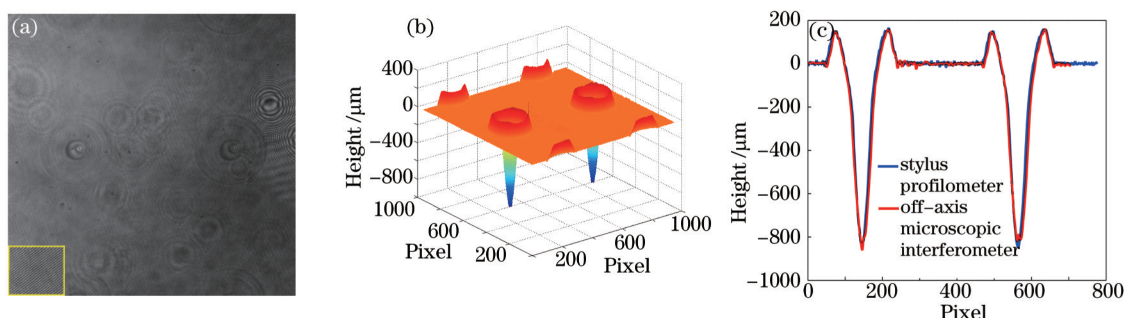

Fig.4 Experimental results for the micro-hole array. (a) Interferogram of the micro-hole array; (b) surface profile of the corrected micro-hole array; (c) profiles of the black line in Fig. 4(b) with the stylus profilometer (dashed dotted line) and the off-axis microscopic interferometer (solid line)

In classical microscopic interferometry, the carrier frequency can be increased by tilting the specimen. However, the phase extracted from such an interferogram is actually incorrect because of spectrum aliasing. The micro-hole array was also tested using a Mirau microscopic interferometer combined with Fourier transform. The sample was placed at a small angle to the horizontal plane, which resulted in a slight off-axis effect being achieved. The results obtained are shown in Fig. 5.

In Fig. 5(a), the spacing between the interference fringes is much larger than that shown in Fig. 3(a) and Fig. 4(a), which means that the carrier frequency is lower. Fig. 5(b) reveals that the virtual image and real image parts are mixed with the zero-order diffraction term. Thus, the surface profile shown in Fig. 5(c) is incorrect. Fig. 5(d) shows the interferogram with a slightly tilted angle of 10° between the plane of the sample and the horizontal plane. The smaller spacing between the interference fringes in Fig. 5(d) shows that the carrier frequency has increased. The real image or virtual image term is separated from the zero-order diffraction term in frequency spectrum after filtering, as described in section 2. The phase is shown in Fig. 5(f). However, the surface profile obtained is incorrect because the frequency spectrum is still overlapped, which results in the information after filtering being incomplete. Furthermore, the area tested is too small. In contrast, the effective area of the field of view of the off-axis microscopic interferometry can be full field.

The above results validate the feasibility of off-axis microscopic interferometry. It is clear that the off-axis microscopic interferometry can be applied to microstructures with more complicated surface profiles than those to which classical microscopic interferometry combined with the Fourier transform method is applicable.

4 Conclusions

This paper proposed a technique for realization of phase retrieval from only one interferogram using off-axis microscopic interferometry. Compared to classical microscopic interferometry, the interferogram obtained has a sufficiently high carrier frequency to assure correct filtering in the Fourier plane via the Fourier transform method. The experimental results obtained for the step height standard and micro-hole array are in good agreement with those obtained using a stylus profilometer, indicating that the technique is valid. A comparative test conducted with

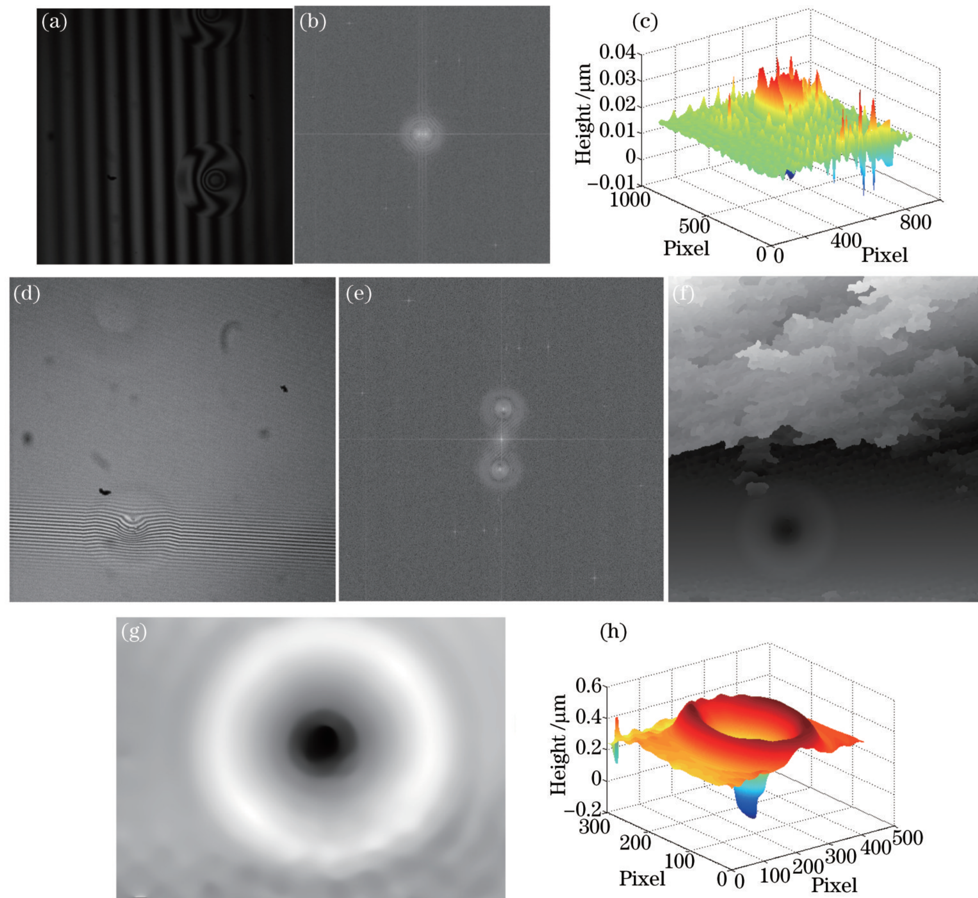

Fig.5 Experimental results obtained using classical microscopic interferometer. (a) Interferogram of micro-hole array (without tilting) for a Mirau microscopic interferometer; (b) frequency spectrum of Fig. 5(a); (c) three-dimensional height distribution of the filtered interferogram shown in Fig. 5(a); (d) interferogram of micro-hole array with a slightly tilted angle of 10°; (e) frequency spectrum of Fig. 5(d); (f) phase extracted from the filtered interferogram shown in Fig. 5(d); (g) effective part of Fig. 5(f); (h) three-dimensional height distribution of Fig. 5(g)

a Mirau interferometric microscope shows that the carrier frequency can be increased by tilting the specimen in classical microscopic interferometry. However, the phase extracted from such an interferogram is incorrect because of spectrum aliasing. Thus, off-axis microscopic interferometry can be applied to microstructures with more complicated surface profiles than those to which classical microscopic interferometry combined with the Fourier transform method is applicable. Because only one interferogram is needed, off-axis microscopic interferometry has the advantage of high efficiency, full field-of-view, and vibration-immunity for measurements. Further, its microscopic objective maintains long working distance. This method also facilitates observation and measurement of dynamic processes.

References

1 Pryputniewicz R J. Holography[M]. //Springer Handbook of Experimental Solid Mechanics. New York: Springer, 2008: 675-700.

2 Yang L, Ettemeyer A. Strain measurement by three-dimensional electronic speckle pattern interferometry: Potentials, limitations, and applications[J]. Optical Engineering, 2003, 42(5): 1257-1266.

3 Post D, Han B, Moiré interferometry[M]. //Springer Handbook of Experimental Solid Mechanics. New York: Springer, 2008: 627-654.

4 Nelson D V. Residual stress determination by hole drilling combined with optical methods[J]. Experimental Mechanics, 2010, 50(2): 145-158.

5 Lin C S, Loh G H, Fu S H, *et al.*. An automatic evaluation method for the surface profile of a microlens array using an optical interferometric microscope[J]. Measurement Science and Technology, 2010, 21(10): 105304.

6 Petitgrand S, Bosseboeuf A. Simultaneous mapping of out-of-plane and in-plane vibrations of MEMS with (sub)nanometer resolution

[J]. Journal of Micromechanics and Microengineering, 2004, 14(9): S97.

7 Nolte D. Interference microscopy[M]. //Optical Interferometry for Biology and Medicine. New York: Springer, 2012: 251-272.

8 Chen F, Brown G M, Song M. Overview of three-dimensional shape measurement using optical methods[J]. Optical Engineering, 2000, 39(1): 10-22.

9 Windecker R, Fleischer M, Körner K, *et al.*. Testing micro devices with fringe projection and white-light interferometry[J]. Optics and Lasers in Engineering, 2001, 36(2): 141-154.

10 Guo T, Zhang Y, Wang S, *et al.*. Micro- structure characterization based on white light interferometry[C]. 2012 International Workshop on Image Processing and Optical Engineering, 2012: 833509.

11 Wang Z, Han B. Advanced iterative algorithm for phase extraction of randomly phase- shifted interferograms[J]. Optics Letters, 2004, 29(14): 1671-1673.

12 Marroquin J L, Servin M, Rodriguez Vera R. Adaptive quadrature filters for multiple phase- stepping images[J]. Optics Letters, 1998, 23(4): 238-240.

13 Larkin K. A self- calibrating phase- shifting algorithm based on the natural demodulation of two- dimensional fringe patterns[J]. Optics Express, 2001, 9(5): 236-253.

14 Osten W. Optical Inspection of Microsystems[M]. Boca Raton: CRC Press, 2006: 376.

15 Ikeda T, Popescu G, Dasari R R, *et al.*. Hilbert phase microscopy for investigating fast dynamics in transparent systems[J]. Optics Letters, 2005, 30(10): 1165-1167.

16 Jang J, Bae C Y, Park J K, *et al.*. Self-reference quantitative phase microscopy for microfluidic devices[J]. Optics Letters, 2010, 35(4): 514-516.

17 Popescu G, Ikeda T, Dasari R R, *et al.*. Diffraction phase microscopy for quantifying cell structure and dynamics[J]. Optics Letters, 2006, 31(6): 775-777.

18 Hu X, Liu G, Hu C, *et al.*. Characterization of static and dynamic microstructures by microscopic interferometry based on a Fourier transform method[J]. Measurement Science and Technology, 2006, 17(6): 1312.

19 Srivastava V, Anna T, Mehta D S. Full-field Hilbert phase microscopy using nearly common-path low coherence off-axis interferometry for quantitative imaging of biological cells[J]. Journal of Optics, 2012, 14(12): 125707.

20 Garcia-Sucerquia J, Ramírez J A H, Prieto D V. Reduction of speckle noise in digital holography by using digital image processing [J]. Optik-International Journal for Light and Electron Optics, 2005, 116(1): 44-48.

21 Cuche E, Marquet P, Depeursinge C. Aperture apodization using cubic spline interpolation: Application in digital holographic microscopy [J]. Optics Communications, 2000, 182(1): 59-69.

22 Schlichthaber F, von Bally G, Kemper B. Influence of Fresnel diffraction on numerical propagation and correction of tilted image planes in digital holographic microscopy[C]. SPIE, 2012, 8430: 843003.

23 Schnars U, Jüptner W. Direct recording of holograms by a CCD target and numerical reconstruction[J]. Applied Optics, 1994, 33(2): 179-181.

24 Schnars U, Jüptner W P O. Digital recording and numerical reconstruction of holograms[J]. Measurement Science and Technology, 2002, 13(9): R85.

25 Weng J, Zhong J, Hu C. Digital reconstruction based on angular spectrum diffraction with the ridge of wavelet transform in holographic phase-contrast microscopy[J]. Optics Express, 2008, 16(26): 21971-21981.

栏目编辑: 吴秀娟